Thin Solid Films 518 (2010) 3782–3785

Contents lists available at ScienceDirect

Thin Solid Films

journal homepage: www.elsevier.com/locate/tsf

Nanocone SiGe antireflective thin films fabricated by ultrahigh-vacuum chemical vapor deposition with *in situ* annealing

Yuan-Ming Chang [a], Ching-Liang Dai [a,*], Tsung-Chieh Cheng [b], Che-Wei Hsu [c]

[a] Department of Mechanical Engineering, National Chung Hsing University, Taichung, 402 Taiwan, ROC
[b] Department of Mechanical Engineering, National Kaohsiung University of Applied Science, Kaohsiung, 415 Taiwan, ROC
[c] Department of Mechanical Engineering, National Chiao Tung University, Hsinchu, 300 Taiwan, ROC

ARTICLE INFO

Article history:
Received 29 May 2008
Received in revised form 18 September 2009
Accepted 23 December 2009
Available online 11 January 2010

Keywords:
SiGe
Thin films
Annealing
Nanostructures
Antireflective layer
Atomic force microscopy

ABSTRACT

In this study, we fabricated nanocone-presenting SiGe antireflection layers using only ultrahigh-vacuum chemical vapor deposition. *In situ* thermal annealing was adopted to cause SiGe clustering, yielding a characteristic nanocone array on the SiGe surface. Atomic force microscopy indicated that the SiGe nanocones had uniform height and distribution. Spectrophotometric measurements revealed that annealing at 900 °C yielded SiGe thin films possessing superior antireflective properties relative to those of the as-grown SiGe sample. We attribute this decrease in reflectance to the presence of the nanostructured cones. Prior to heat treatment, the mean reflectance of ultraviolet rays (wavelength < 400 nm) of the SiGe thin film was ca. 61.7%; it reduced significantly to less than 28.5% when the SiGe thin film was annealed at 900 °C. Thus, the drop in reflectance of the SiGe thin film after thermal treatment exceeded 33%.

1. Introduction

SiGe thin films have attracted considerable attention because of their high electron and hole mobilities [1–3]. The preparation of these films is compatible with Si-based technologies, which have been used to fabricate high-performance optoelectronic SiGe devices, such as optical modulators [4] and field effect transistors [5]. Although SiGe thin films also have potential as components of highly efficient solar cells [6,7], reflection loss, which occurs when the cell surface reflects much of the incident light, is a serious issue that severely reduces their efficiency. Thus, an effective approach for the fabrication of antireflective thin films is required if we are to manufacture high-efficiency solar cells and optoelectronic devices.

Many methods have been developed for manufacturing SiGe thin films featuring antireflective patterns. For instance, Brammer et al. [8], and Forniés et al. [9] obtained thin films with antireflective patterns by wet etching using hydrochloric acid and nitric acid, respectively. Nositschka et al. [10] used reactive ion etching to produce multicrystalline Si displaying an antireflective pattern on a solar cell. Hattori [11] introduced polymer particles to cause destructive interference and, thereby, reduce reflectance. Nevertheless, such schemes suffer either from chemical contamination or the need for an excessive fabrication period.

In this study, we fabricated nanocone-presenting SiGe antireflective thin films using *in situ* thermal annealing. This approach has several significant advantages. First, contamination of the SiGe thin films is entirely prevented because the films do not come into contact with any impurities during the fabrication and annealing processes; therefore, accurate data on the films can be obtained (e.g., variations in structural properties following thermal treatment). Second, heat treatment is a simple procedure that takes only a small fraction of the fabrication time required for batch-produced devices. Finally, thermal annealing is fully compatible with Si-based technologies. Nanocone SiGe thin films themselves have several attractive features that make them suitable for numerous applications. For example, they have ultraviolet (UV)-antireflective properties, which can increase the efficiency of SiGe-based solar cells. In this study, we used transmission electron microscopy (TEM), high-resolution X-ray diffraction (HRXRD), atomic force microscopy (AFM), and spectrophotometry to measure the properties of SiGe thin films. We found that the mean reflectance of the SiGe thin films for UV rays reduced from 61.7 to 28.5% after annealing at 900 °C.

2. Experimental details

SiGe epitaxial thin films were grown onto 6-inch p-type Si (100) in an ultrahigh-vacuum chemical vapor deposition (UHVCVD) system (ANELVA SRE-612, Japan) [12,13]. The Si wafers had undergone standard cleaning according to the guidelines of the Radio Corporation of America (RCA) [14]; they were dipped in dilute hydrofluoric acid to

* Corresponding author.
E-mail address: cldai@dragon.nchu.edu.tw (C.-L. Dai).

0040-6090/$ – see front matter © 2010 Elsevier B.V. All rights reserved.
doi:10.1016/j.tsf.2009.12.105

passivate their surfaces. As a result, when the wafers were transported through air and introduced into the loadlock chamber of the UHVCVD system, their surfaces remained cleaned [15]. As soon as the system temperature was increased to 550 °C, and the deposition chamber was pumped to 1.6×10^{-7} Pa using a turbo molecular pump, the wafers were transferred directly to the deposition chamber from the loadlock chamber. The inlet gases were a mixture of Si_2H_4 at a flow rate of 1 sccm and GeH_4 at a flow rate of 7 sccm. SiGe epitaxial thin films were grown at a total growth rate of 8.04 nm/min. Following the growth of the thin film, *in situ* thermal annealing was performed at 700, 800, and 900 °C for 15 min in the UHVCVD chamber.

Cross-sectional TEM images of thin films were obtained using a transmission electron microscope (JEOL JEM-2010F, Japan) with an operating voltage of 200 kV; the compositions of thin films were verified using energy-dispersive X-ray spectroscopy (EDS). HRXRD (PANalytical X'Pert Pro, Singapore) with Cu Kα radiation ($\lambda = 0.154$ nm) was applied to determine the phase formation and the crystallographic structure of all samples. A hybrid monochromator and a triple-axis X-ray diffractometer were adopted in a high-resolution Gonio scan (θ–2θ) and in high-resolution reciprocal space mapping (HRRSM) to observe the structural features of the SiGe thin films. Tapping-mode AFM (Veeco Dimension 5000, USA) was used to image the surface morphologies of the SiGe thin films at a constant frequency of 1.0 Hz. The reflectivity of the SiGe epilayers was measured using a spectrophotometer (Jasco V-670, Japan) and unpolarized light of wavelengths ranging from 200 to 800 nm. To obtain precise information on the optical properties of the nanopatterned SiGe thin films, an integrating sphere was applied in the spectrophotometer to determine the total reflectance; theory of integrating spheres was well presented by Jacquez et al. [16]. The optical configuration of the spectrophotometer is presented in Fig. 1, where *D* represents the light source of wavelengths in the range 200–700 nm; *W* is the light sources of wavelengths of greater than 700 nm; *S* is the slit; and *G* is the grating. The sample is set in close proximity to the integrating sphere, and the detector that is part of the integrating sphere assembly is utilized to detect the optical reflectance.

3. Results and discussion

Fig. 2(a) presents a cross-sectional TEM image of the as-deposited SiGe epitaxial thin film. The SiGe layer was 102 nm thick with a Si (100) orientation. The EDS analysis revealed that the thin film was composed of Si and Ge elements. The Ge content of the SiGe epilayers was ca. 25% prior to annealing. The high-resolution TEM image of the as-grown SiGe epitaxial thin film indicates that it had a highly textured structure, produced by the UHVCVD system. The diffraction pattern from within the SiGe thin film prior to annealing (inset to Fig. 2(b)) reveals that the incident electron beam formed the brightest spot near the center, which is in the (110) crystallographic direction.

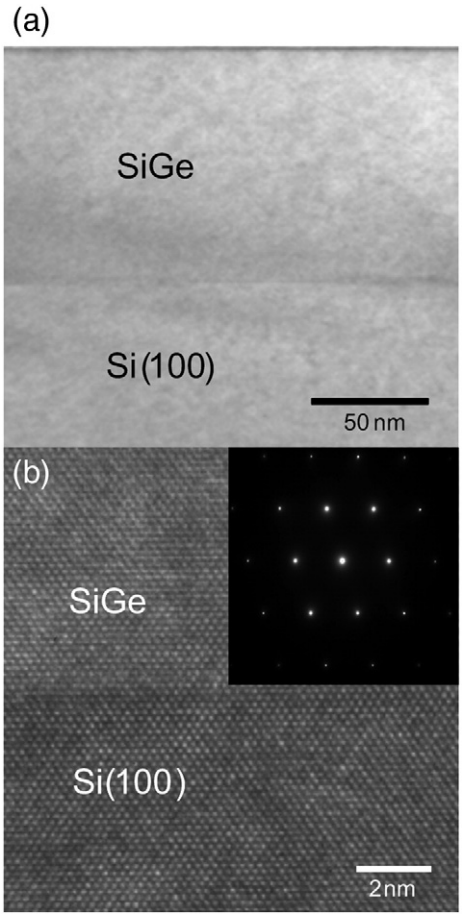

Fig. 2. (a) Cross-sectional TEM image of the as-grown SiGe/Si (100) heterostructure. (b) High-resolution TEM image and (inset) diffraction pattern of the as-deposited SiGe thin film.

We used HRXRD analysis to characterize the crystallographic structure of the SiGe thin film. Fig. 3 displays the XRD curves of the (0 0 4) reflections from SiGe thin films that had been annealed at various annealing temperatures. The curve of the as-grown film had two sharp peaks: one at 69.12° was from the Si substrate and the other

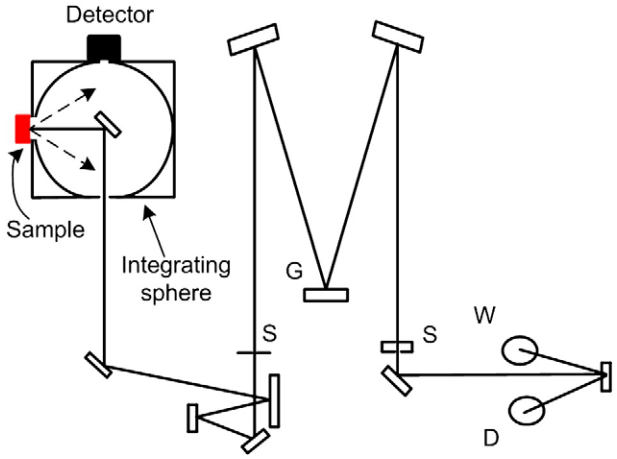

Fig. 1. Schematic representation of the optical configuration in the spectrophotometer.

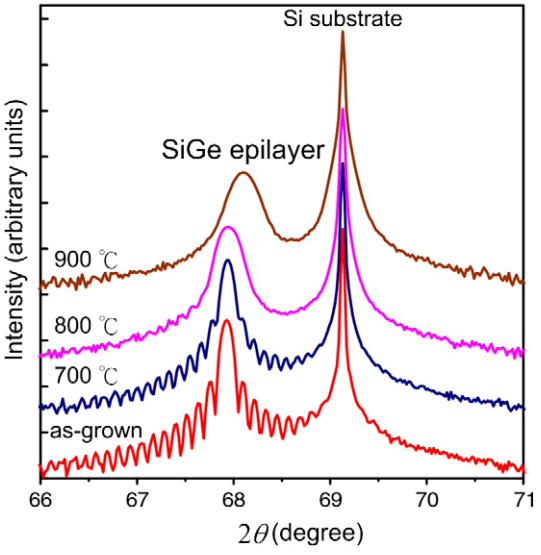

Fig. 3. XRD curves of SiGe thin films prepared at various annealing temperatures.

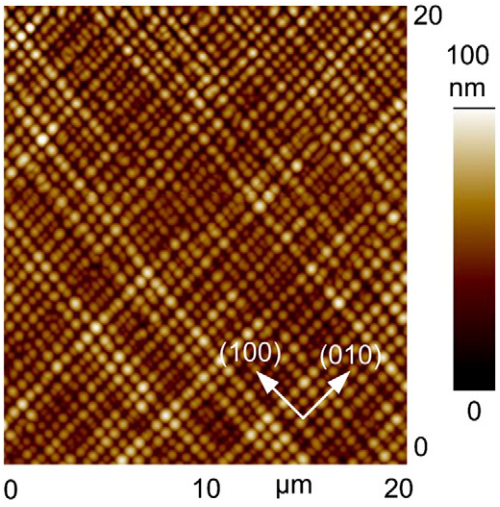

Fig. 4. Two-dimensional AFM image of the SiGe thin film that had been annealed at 900 °C.

at 67.92° represented the SiGe film. The SiGe signal of the film that had been annealed at 700 °C was slightly shifted to the higher angle; annealing at 900 °C shifted the SiGe peak further to 68.10°. This change in the SiGe peak position proves that the film underwent strain relaxation during thermal annealing [17]. Moreover, the sharp peak for the SiGe sample disappeared gradually upon increasing the thermal annealing temperature as a result of the interface broadening due to the interdiffusion between the thin film and the Si substrate. That is to say, the interface changed during high-temperature thermal annealing [18]. Based on HRRSM analyses, the as-grown SiGe sample was fully strained, and the relaxed degree of sample that had been annealed at 900 °C was 36.1%.

We used AFM to measure the surface morphology of the SiGe thin film. Fig. 4 displays the surface morphology of the SiGe film (two-dimensional AFM image) that had been annealed at 900 °C. The uniformly distributed nanostructures are clearly visible on the SiGe surface. We attribute the structural deformation to the fact that the lattice mismatch between Si and SiGe produced a misfit dislocation network at the interface between the SiGe epilayer and the Si substrate [19]. Thermal annealing introduced the misfit dislocation network into the SiGe layer, causing structural deformation in the thin film. Because all the individual cells in the network had similar geometries and were aligned perpendicular to the adjacent ones, the nanocones had similar geometries and lay perpendicular on the SiGe surface. Moreover, the nanocones were separated by grooves in the (100) and (010) directions as a result of the thin film having been deposited on the Si (100) substrate. Hence, the nanocone topography of the SiGe surface was obtained after thermal annealing at 900 °C; the root mean square (rms) roughness of this film was ca. 15.5 nm. The type of roughness observed in this study differed from that obtained in previous studies [20–23]. Notably, the as-grown SiGe samples in Refs. [20–23] were partially strain-relaxed because their thickness exceeded the critical value, causing a crosshatched appearance of their surfaces. In our present study, the as-grown SiGe layer was fully strained and the dislocation network was introduced into the thin film through thermal annealing; therefore, the type of roughness differed from that reported previously.

We employed AFM bearing analysis to evaluate the height distribution of the nanostructures on the SiGe thin film. Fig. 5 displays the bearing analysis of the SiGe thin film. In this investigation, we measured $20\times20\ \mu m^2$ areas of the SiGe films that had been processed at different annealing temperatures. Fig. 5(a) presents the bearing analysis of the SiGe film prior to annealing. The convex structures on the film surface are rare; this film was essentially flat. Fig. 5(b) presents the bearing analysis of the SiGe film after annealing at 700 °C; only a few convex structures appear on the surface. Fig. 5(c) and (d) displays the bearing analyses of the SiGe films after annealing at 800 and 900 °C,

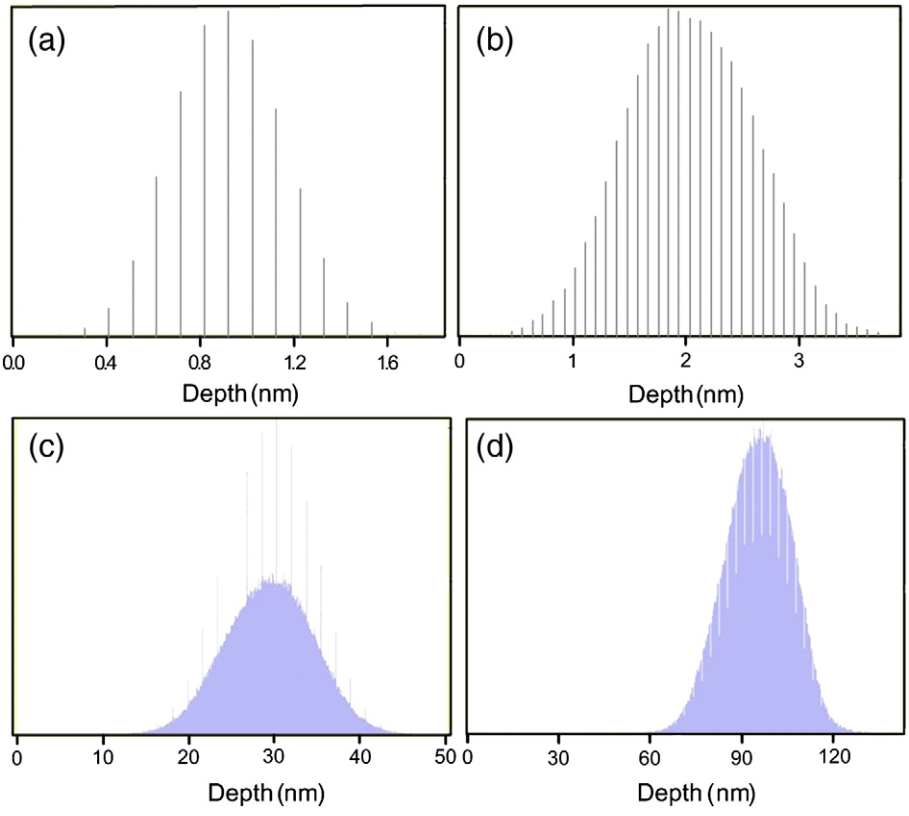

Fig. 5. Bearing analyses of the SiGe thin films (a) before and (b–d) after annealing at (b) 700, (c) 800, and (d) 900 °C.

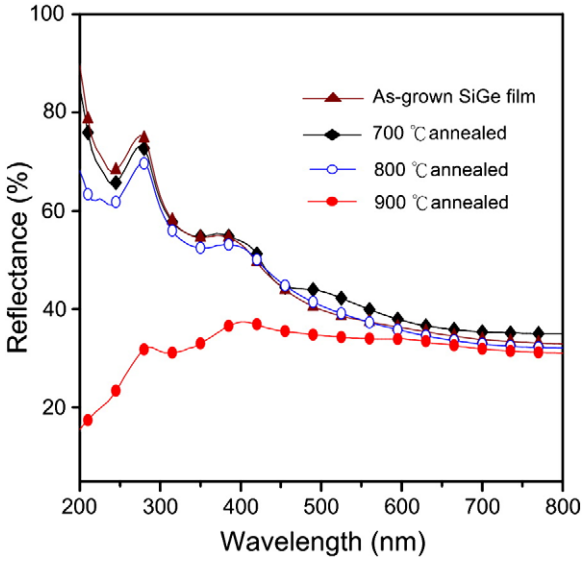

Fig. 6. Reflectance curves of the SiGe samples before and after annealing at 700, 800, and 900 °C.

respectively; the latter presented nanostructures on the SiGe surface that had the greatest height among all of the fabricated SiGe samples.

Figs. 4 and 5 reveal that the SiGe nanocones were of uniform height and were distributed uniformly after annealing at 900 °C. Shieh et al. [24] reported a pyramidal array having antireflective properties, which were exploited in several applications. For instance, an antireflective layer not only increased the efficiency of solar cells, but also reduced the number of ghost images, which can greatly limit the accuracy of micro sun sensors [25]. In this study, we measured the reflectance of the SiGe thin films using a spectrophotometer analyzer. Fig. 6 displays the reflectance curves, at wavelengths ranging from 200 to 800 nm, of the SiGe thin films, before heat treatment and after annealing at 700, 800, and 900 °C. Prior to thermal treatment, the mean reflectance was as high as 61.7% for UV rays of less than 400 nm. The reflectance curve of the as-grown SiGe thin film was almost entirely coincident with the reflectance curve of the SiGe thin film that had been annealed at 700 °C, because the very smooth surface morphologies of these two thin films were similar (low roughness values of 0.3 and 0.6 nm, respectively). The reflectance of the thin film that had been annealed at 800 °C was reduced slightly. Although the surface of the thin film featured nanostructures after annealing at 800 °C, as shown in Fig. 5(c), these nanostructures lacked sufficient height to have any effect on the reflectance, which remained as high as 57.9% at wavelengths from 200 to 400 nm. Following annealing at 900 °C, the reflectance was ca. 28.5% for incident light having wavelengths of less than 400 nm—i.e., more than 33% lower than the reflectance of the as-grown SiGe thin film for UV rays. Thus, the nanostructures effectively reduced the reflective losses and promoted the trapping of UV rays. Interestingly, the layer of SiGe nanocones was very thin (102 nm), making it suitable for use in the manufacturing of optoelectronic devices.

When Nishimoto and Namga [26] applied a wet etching of a monocrystalline Si wafer with Na_2CO_3 (15 wt.%) and NaOH (25 g) for 10 min at 95 °C, they obtained a reflectance for the texture-etched Si substrate of 35.7% in the wavelength range 400–1100 nm. Minemoto et al. [27] employed a coating method to obtain a CdS/glass substrate exhibiting a reflectance of ca. 25% for wavelengths less than 1200 nm. Lee et al. [25] used RIE to fabricate a Si nanotips antireflection surface, the reflectance of which was ca. 8.0% at the target wavelength of 1 μm. In our present study, the average reflectance in the wavelength range from 200 to 800 nm was 33.5%.

4. Conclusion

We have used UHVCVD and *in situ* thermal annealing to fabricate nanocone-presenting SiGe antireflective thin films as a result of SiGe clustering on SiGe surfaces. The mean reflectance of the as-grown SiGe film toward UV rays was as high as 61.7%. The mean reflectance of the film that had been annealed at 900 °C had decreased to 28.5% as a result of the presence of the nanocone array on its surface. Thus, the nanostructures had antireflective properties superior to those of the as-grown sample; i.e., the nanocone array on the SiGe surface effectively reduced reflection losses and enhanced light trapping.

Acknowledgements

The authors would like to thank Dr. Jiann Shieh and Shih-Chiang Chuang for useful discussions, Fu-Kuo Hsueh for UHVCVD, Chiung-Chih Hsu for TEM and Jie-Yi Yao for XRD, and Mei-Yi Liao for spectrophotometric in National Nano Device Laboratories (NDL) and National Science Council of the Republic of China for financially supporting this research under Contract no. NSC 95-2221-E-005-043-MY2.

References

[1] Z. Cheng, J. Jung, M.L. Lee, A.J. Pitera, J.L. Hoyt, D.A. Antoniadis, E.A. Fitzgerald, Semicond. Sci. Technol. 19 (2004) L48.
[2] R. Oberhuber, G. Zandler, P. Vogl, Phys. Rev. B 58 (1998) 9941.
[3] N. Sugii, K. Nakagawa, S. Yamaguchi, M. Miyaob, Appl. Phys. Lett. 75 (1999) 2948.
[4] J. Xiang, W. Lu, Y. Hu, Y. Wu, H. Yan, C.M. Lieber, Nat. Lett. 441 (2006) 489.
[5] Y.H. Kuo, Y.K. Lee, Y. Ge, S. Ren, J.E. Roth, T.I. Kamins, D.A.B. Miller, J.S. Harris, Nat. Lett. 437 (2005) 1334.
[6] M. Tayanagi, N. Usami, W. Pan, K. Ohdaira, K. Fujiwara, Y. Nose, K. Nakajima, J. Appl. Phys. 101 (2007) 054504.
[7] N. Usami, Y. Azuma, T. Ujihara, G. Sazaki, K. Nakajima, Y. Yakabe, T. Kondo, S. Koh, Y. Shiraki, B. Zhang, Y. Segawa, S. Kodama, Appl. Phys. Lett. 77 (2000) 3565.
[8] T. Brammer, W. Reetz, N. Senoussaoui, O. Vetterl, O. Kluth, B. Rech, H. Stiebig, H. Wagner, Sol. Energy Mater. Sol. Cells 74 (2002) 469.
[9] E. Forniés, C. Zaldo, J.M. Albella, Sol. Energy Mater. Sol. Cells 87 (2005) 583.
[10] W.A. Nositschka, C. Beneking, O. Voigt, H. Kurz, Sol. Energy Mater. Sol. Cells 76 (2003) 155.
[11] H. Hattori, Adv. Mater. 13 (2001) 51.
[12] L. Zhang, E. Deckhardt, A. Weber, C. Schönenberger, D. Grützmacher, Nanotechnology 16 (2005) 655.
[13] T.H. Loh, H.S. Nguyen, C.H. Tung, A.D. Trigg, G.O. Lo, N. Balasubramanian, D.L. Kwong, S. Tripathy, Appl. Phys. Lett. 90 (2007) 092108.
[14] P.V. Zant, Mirochip Fabrication, 5th, McGraw-Hill, Boston, 2004, p. 126.
[15] E.V. Thomsen, C. Christensen, C.R. Andersen, E.V. Pedersen, P.N. Egginton, O. Hansen, J.W. Petersen, Thin Solid Film 294 (1997) 72.
[16] J.A. Jacquez, H.F. Kuppenheim, J. Opt. Soc. Am. 45 (1955) 460.
[17] S. Zheng, M. Mori, T. Tambo, C. Tatsuyama, J. Mater. Sci. 42 (2007) 5312.
[18] S. Zheng, M. Kawashima, M. Mori, T. Tambo, C. Tatsuyama, Thin Solid Films 508 (2006) 156.
[19] Y.H. Xie, S.B. Samavedam, M. Bulsara, T.A. Langdo, E.A. Fitzgerald, Appl. Phys. Lett. 71 (1997) 3567.
[20] E.A. Fitzgerald, Y.H. Xie, D. Monroe, P.J. Silverman, J.M. Kuo, A.R. Kortan, F.A. Thiel, B.E. Weir, J. Vac. Sci. Technol. B 10 (1992) 1807.
[21] J. Tersoff, F.K. LeGoues, Phys. Rev. Lett. 72 (1994) 3570.
[22] M.A. Lutz, R.M. Feenstra, F.K. LeGoues, P.M. Mooney, J.O. Chu, Appl. Phys. Lett. 66 (1995) 724.
[23] T. Spila, P. Desjardins, J.D. Gall, R.D. Twesten, J.E. Greene, J. Appl. Phys. 93 (2003) 1918.
[24] J. Shieh, C.H. Lin, M.C. Yang, J. Phys. D: Appl. Phys. 40 (2007) 2242.
[25] C. Lee, S.Y. Bae, S. Mohrab, H. Manohara, Nano Lett. 5 (2005) 2438.
[26] Y. Nishimoto, K. Namga, Sol. Energy Mater. Sol. Cells 61 (2000) 393.
[27] T. Minemoto, M. Murozonz, Y. Yamahuchi, H. Takakura, Y. Hamayaka, Sol. Energy Mater. Sol. Cells 90 (2006) 2995.